Available online at www.sciencedirect.com
ScienceDirect
Biomaterials 28 (2007) 162–174
Biomaterials
www.elsevier.com/locate/biomaterials

Spectroscopic translation of cell–material interactions

Josephine Allen, Yang Liu, Young L. Kim, Vladimir M. Turzhitsky, Vadim Backman, Guillermo A. Ameer*

Northwestern University, Biomedical Engineering Department, 2145 Sheridan Rd., Room E310, Evanston, IL 60208, USA

Received 21 April 2006; accepted 5 July 2006
Available online 1 August 2006

Abstract

The characterization of cellular interactions with a biomaterial surface is important to the development of novel biomaterials. Traditional methods used to characterize processes such as cellular adhesion and differentiation on biomaterials can be time consuming, and destructive, and are not amenable to quantitative assessment in situ. As the development of novel biomaterials shifts towards small-scale, combinatorial, and high throughput approaches, new techniques will be required to rapidly screen and characterize cell/biomaterial interactions. Towards this goal, we assessed the feasibility of using 4-dimensional elastic light-scattering fingerprinting (4D-ELF) to describe the differentiation of human aortic smooth muscle cells (HASMCs), as well as the adhesion, and apoptotic processes of human aortic endothelial cells (HAECs), in a quantitative and non-perturbing manner. HASMC and HAEC were cultured under conditions to induce cell differentiation, attachment, and apoptosis which were evaluated via immunohistochemistry, microscopy, biochemistry, and 4D-ELF. The results show that 4D-ELF detected changes in the size distributions of subcellular organelles and structures that were associated with these specific cellular processes. 4D-ELF is a novel way to assess cell phenotype, strength of adhesion, and the onset of apoptosis on a biomaterial surface and could potentially be used as a rapid and quantitative screening tool to provide a more in-depth understanding of cell/biomaterial interactions.

Keywords: Light scattering; Optics; Tissue engineering; Cell characterization; Cell morphology; Cell–substrate interaction

1. Introduction

Current methods to monitor cell adhesion, apoptosis and phenotypic differentiation on materials for tissue engineering include techniques such as histology, confocal-microscopy, RT-PCR, biochemical assays, and flow cytometry. Although commonly used in biomaterials research, these techniques can be destructive, often include artifacts due to preparation protocols, are time consuming, and often times are costly, particularly if many materials must be tested for their cell compatibility properties. With the advent of combinatorial approaches to the development of biomaterials, there is a need for accessible technologies that can rapidly provide a real-time, non-perturbing, quantitative assessment of cell–material interactions. Although based on different sensing principles, some examples of technologies or approaches that have been useful in assessing tissue microarchitecture include electrical cell–substrate impedance sensing (ECIM) [1], quartz crystal microscopy (QCM) [1], optical waveguide lightmode spectroscopy (OWLS) [1], optical coherence tomography [2], fluorescence spectroscopy, Raman spectroscopy [3,4], and angle-resolved low-coherence interferometry [5]. Collectively these techniques are a step in the right direction; however, they may still require some degree of sample preparation or modification prior to analysis.

A recently developed enhancement of light-scattering spectroscopy (LSS), referred to as 4-dimensional elastic light-scattering fingerprinting (4D-ELF), has been shown to discriminate between cancerous and normal cells by detecting and analyzing light back-scattered from subcellular structures [6]. LSS-based imaging has been shown to provide a quantitative assessment of subcellular events, such as organelle enlargement or increased chromatin content, in a real-time and non-destructive manner [7–12].

*Corresponding author. Tel.: +1 847 467 6719; fax: +1 847 491 4928.
E-mail address: g-ameer@northwestern.edu (G.A. Ameer).

0142-9612/$ - see front matter © 2006 Elsevier Ltd. All rights reserved.
doi:10.1016/j.biomaterials.2006.07.002

Light-scattering signals are rich in information yielding unprecedented insights into the micro-architectural organization of cells interacting with substrates. The spectral analysis of light scattered by living tissues provides information about the size scale of internal structures within the cell. Light-scattering signals depend on the size, shape, and organization of intracellular structures, and are sensitive not only to the "scatterer" but also the immediate surrounding milieu (i.e. the concentration of solid particles, such as proteins) [13].

We hypothesize that interfacial cell/biomaterial interactions will affect sub-cellular structures in defined ways, giving rise to specific light-scattering "fingerprints" that can be used to describe an ongoing cellular process. Specifically, interactions during the process of cell attachment onto a substrate can be assessed through the possible detection of changes in cell shape [14,15], sub-cellular organelle distribution [16], nuclear deformation [17], focal adhesion complex formation [18–20], and the assembly of micro-filamentous stress fibers [18–20]. Interactions involved in phenotypic differentiation could be assessed through the possible detection of changes in organelle size, abundance, and distribution as well as the abundance of actin and myosin filaments [21–26]. Interactions resulting in cell death via apoptosis can also be assessed, through the possible detection of nuclear chromatin condensation, cytoplasmic shrinking, and changes in size and shape of the cell nuclei and cell cytoplasm [12,27,28].

The work presented herein describes how 4D-ELF can potentially allow the identification of vascular SMC and EC differentiation processes, based on characteristic 4D-ELF spectral fingerprints. A comparison of the 4D-ELF profiles of cultured vascular cells can provide a quick and easy means to monitor cellular growth and differentiation on new biomaterials, once these processes have been calibrated. Ultimately, the microstructure of the cells can be quantified to determine if the scaffold environment supports cellular attachment, growth, retention, proliferation, and healthy tissue formation.

2. Experimental

2.1. Assessment of cell differentiation

Human aortic smooth muscle cells (SMCs) (Cambrex, East Rutherford, NJ) were induced to a uniform state of either contractile or proliferative phenotypes by culturing them on glass cover slips coated with either 25 μg/ml laminin or 25 μg/ml fibronectin, respectively. SMCs were cultured in SM-basal media (SmBM), supplemented with human epidermal growth factor (hEGF), human fibroblast growth factor (hFGF), gentamicin/amphotericin-B (GA-1000), insulin, and 5% fetal bovine serum (FBS). Cells were cultured at 37 °C, 95% relative humidity, and 5% CO_2 for 5–11 days. Once the phenotypes were achieved, immunohistochemistry was done using primary antibodies to smooth muscle cell specific marker, smooth muscle α-actin (SM-α-actin). (Sigma Aldrich, Milwaukee, WI) SMC proliferation was assessed by incubating the cells grown on both laminin and fibronectin with culture media containing fluorescently labeled 5-bromo-2′-deoxy-uridine (BrDU). BrDU incorporates into newly synthesized DNA, and thus is an indicator of cell proliferation. The cells that incorporated BrDU were visualized via fluorescence microscopy.

2.2. Assessment of cell adhesion

Human aortic endothelial cells (HAECs) (Cambrex, East Rutherford, NJ) were cultured in EC basal media-2 (EBM-2), supplemented with hEGF, hydrocortisone, GA-1000, vascular endothelial growth factor, hFGF-B, R3-insulin growth factor-1, ascorbic acid, heparin, and 10% FBS, at 37 °C, 95% relative humidity and 5% CO_2 for 15, 30, 60 and 120 min on either 25 μg/ml laminin or fibronectin-coated glass cover slips. Following the attachment time, the HAECs were probed with primary antibodies to focal adhesion complex specific protein vinculin, and actin specific phalloidin (Chemicon, Temecula, CA) via immunohistochemistry.

The relative strength of adhesion of HAEC to laminin and fibronectin was assessed using a previously described centrifugation assay [29]. The wells of a black 96-well tissue culture polystyrene (TCP) plate were coated with either 25 μg/ml laminin or 25 μg/ml fibronectin. Prior to the assay, the HAEC were fluorescently labeled with membrane permeable Calcein-AM (Invitrogen-Molecular Probes, Carlsbad, CA). Labeled cells were seeded into the wells and allowed to attach to the substrate for the appropriate duration. The plates were subsequently inverted and centrifuged at 750 rpm, applying 72 g detachment force, for 5 min. The fluorescence intensity of each well was read at 494 nm prior to and following the detachment spin.

2.3. Assessment of cell apoptosis

Tumor necrosis factor-α (TNF-α), a pro-apoptotic agent, was used to induce the molecular events that occur in the early stages of apoptosis [30]. Lactate dehydrogenase release (LDH), light microscopy, and measurements of caspase-3 activity were used to assess the physical and biological characteristics of apoptosis. To determine the optimal concentration of TNF-α to induce apoptosis within the experimental time of 3 h, HAECs were cultured in EBM-2 (fully supplemented as described) supplemented with TNF-α (Sigma Aldrich, Milwaukee, WI) at concentrations of 0.1, 0.5, 1.0, 10 and 50 ng/ml. LDH released into the cell culture media due to cell membrane damage was quantified using a cytotoxicity detection kit (Roche Applied Science, Indianapolis, IN) and compared to media samples from cells not exposed to TNF-α.

Subcellular molecular events associated with apoptosis were assessed by detecting caspase-3 activity (Assay design, Anne Arbor, MI) in cell lysates of TNF-α-challenged cells. Following a 3-h incubation with TNF-α, the media was aspirated, the cells were washed with PBS, then lysed in 150 μl of lysis buffer containing 10% protease inhibitor (Sigma Aldrich, Milwaukee, WI) and 1% Triton-X (Sigma Aldrich, Milwaukee, WI). The cell lysate was kept on ice, until assayed for caspase-3 activity. Lysates from cells incubated in media containing no TNF-α served as the baseline control. 4D-ELF analysis was conducted using HAECs that did not demonstrate changes in cytoplasm or cell membrane integrity following exposure to TNF-α. Cell membrane integrity was assessed via light microscopy or the LDH assay.

2.4. Transmission electron microscopy (TEM)

Primary fixation of the SMCs and HAECs was done in 2% paraformaldehyde/2% gluteraldehyde. The cells were post-fixed in 2% osmium tetraoxide, dehydrated in graded ethanol (50–100%), and embedded in Epon resin. Sections were placed on 200 mesh copper grids, stained with uranyl acetate, lead citrate, and viewed on a Jeol 1220 TEM at 80 kV (Research Resources Center, University of Illinois at Chicago, Chicago, IL).

TEM images were quantified for specific structural characteristics. For the assessment of phenotype, the images of SMCs cultured on laminin and fibronectin were examined for the density of key organelles, mitochondria and rough endoplasmic reticulum (RER). The number of each organelle

was counted by visual inspection of five separate TEM images taken at 12,000–40,000 × magnification. All the mitochondria and RER in the field of view of the TEM image were counted and the number was normalized to 10 um^2 of cell surface area. For the assessment of EC attachment study, ECs attached to laminin and fibronectin for 60 and 120 min were examined for the density of electron dense contact points. These contact points were counted by visual inspection of at least 5–8 separate TEM images taken at 20,000–40,000 × magnification. All of the contact points were counted and normalized to 10 um of cell length.

2.5. 4D-ELF experimental setup

The detailed description of the 4D-ELF setup has been described previously, and is shown in Fig. 1 [31,32]. Briefly, the glass cover slip with the attached cells was gently rinsed in Hank's balanced salt solution (HBSS) to remove any media. The cover slip was then immersed in pre-warmed HBSS in a 60 mm glass Petri dish in preparation for 4D-ELF measurements. An area of the cultured cells on the glass cover slip, approximately 1 mm in diameter, was illuminated by a collimated linearly polarized beam of broadband-light emitted by a xenon light source. By means of the analyzing polarizer positioned in the light collection arm of the system, a Fourier lens positioned one focal distance from the sample surface, and the imaging spectrometer coupled to the charge-coupled device (CCD), the instrument records a matrix of the distribution of scattered light intensity for various wavelengths (from 400 to 700 nm) and angles of scattering (within $\pm 8^\circ$ from the backward direction). In this matrix, one axis corresponds to the wavelength of light and the other to the angle of scattering for a fixed polarization and the azimuth of scattering (the polar angle of the direction of light propagation with respect to the direction of polarization). The azimuth of scattering is selected by rotating the polarizer in the delivery arm of the system. The combination of the linear polarizer in the delivery arm of the system and the analyzing polarizer allows measurement of the intensity of two independent components of the light scattered from the cell: scattered light polarized along the direction of polarization of the incident light (co-polarized component $I_{\parallel}$) and the scattered light polarized orthogonally to the polarization of the incident light (the cross polarized component $I_{\perp}$).

To compensate for the non-uniform spectral profile of the light source and other artifacts, the light-scattering intensity maps, referred to as "fingerprints", were normalized to a reflectance standard. The instrument was calibrated as previously described and tested using a conventional protocol with standard polystyrene microspheres of different sizes ranging from 0.2 to 10 um [32]. Representative calibration data can be seen in Fig. 2. For each sample measured, the corresponding substrate was measured as "background"; and this background measurement was subtracted from the sample measurements. The light-scattering data recorded in these experiments were found to be in excellent agreement with the predictions of Mie theory, which provides the exact solution to the light scattering by spheres.

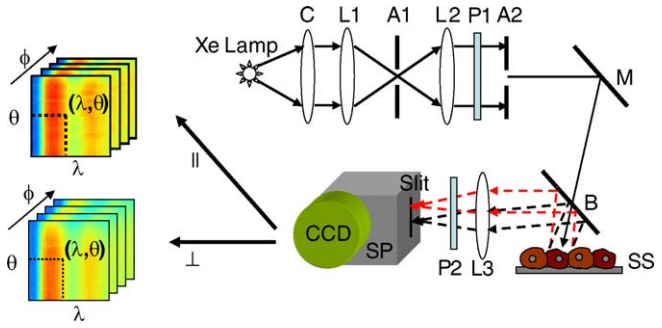

Fig. 1. Schematic representation of 4D-ELF Instrumentation. Xe: xenon lamp, C: condenser, L: lenses, A: apertures, P: polarizer, M: mirrors, B: beam splitter, SS: sample stage, SP: spectrograph, and CCD: CCD camera. Light-scattering fingerprint: 4-D information include scattering angle (θ), wavelength (λ), Azimuthal angle (ϕ), and polarization ($\parallel/\perp$).

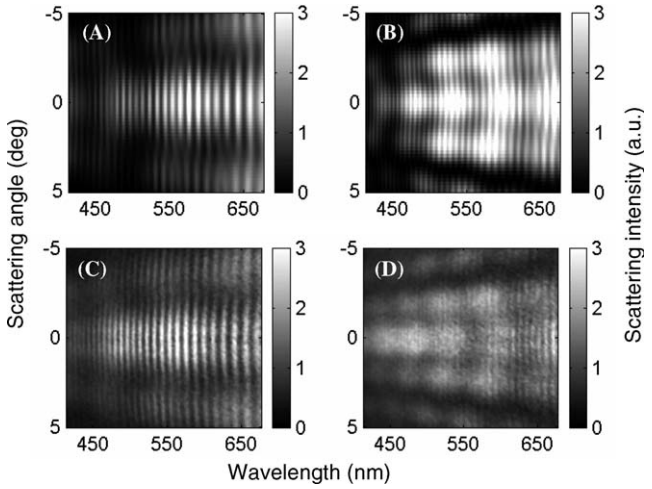

Fig. 2. 4D-ELF calibration data. Images of the predicted light scattered by microspheres with a mean diameter of (A) 5.80 ± 0.2 μm and (B) 9.30 ± 0.3 μm were stimulated using Mie theory. Experimental data using aqueous suspension of polystyrene microspheres with a mean diameter of (A) 5.80 ± 0.2 μm and (B) 9.30 ± 0.3 μm.

4D-ELF records a matrix of information in four dimensions. The four dimensions are (1) wavelength—visible light (400–700 nm); (2) scattering angle—records backscattered light (± 8 degrees); (3) Azimuthal angle—angular difference between the direction of the spectrograph slit and the polarization (P1) direction of the incident beam; (4) polarization—depending on the position of the two polarizers in the system (P1 and P2), the scattered light that co-polarizes or cross-polarizes with the incident beam can be collected.

2.6. 4D-ELF data analysis

Spectral behavior of light scattering depends on the size distribution of scattering structures. The data obtained by 4D-ELF are provided in the form of characteristic "fingerprints" which depict the intensity of the backscattered light, as a function of wavelength and backscattered angle $\pm 8^\circ$. The spectral "fingerprint" data are made linear by plotting the average intensity of the backscattered light across all scattering angles at each wavelength (400–700 nm). Generally, scattering intensity is a declining function of wavelength, and its spectral slope is related to the relative proportion of structures of different sizes. To analyze the data and characterize the spectral variations of $I(\lambda)$, we obtained linear fits to $\log(I(\lambda))$ vs. $\log(\lambda)$ using linear regression analysis. The absolute value of the linear coefficient of the fit (in all measurements the linear coefficient is negative due to the decrease of $I(\lambda)$ with wavelength), is referred to hereafter as the "spectral slope". Typically, larger structures tend to have smaller spectral slopes, whereas smaller structures tend to increase the slope. The spectral slope was obtained for each sample and used in statistical analyses.

To obtain the complete size distribution of cellular and subcellular structures at each site, the spectra computationally simulated using Mie theory were fit to the differential polarization spectra using conventional least-squares minimization algorithm [33]. In each fitting, several types of size distributions (normal, log-normal, or uniform) were assumed. We found that the spectra recorded for near-backward angles had spectral behavior similar to an inverse power-law [8]. When the sizes of the scatterers are widely distributed, which is always the case in biological cells, the log-normal or power-law size distributions provide fits superior to those obtained using a normal or uniform size distribution. The size-sensitivity studies showed that the differential polarization spectra are primarily sensitive only to scatterers whose sizes range from 40 to 800 nm. These limits, therefore, provide the range of validity of the size distributions obtained using the fitting algorithm.

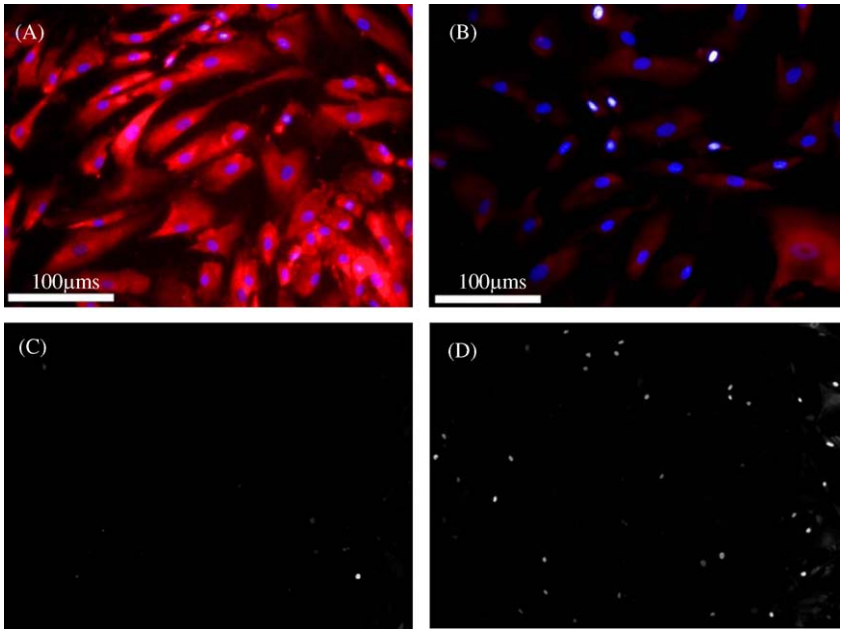

Fig. 3. Smooth muscle cells cultured on (A) laminin and (B) fibronectin-coated TCP were probed for SM-α actin (200 ×). The actin localization is red and the nuclei are labeled blue with DAPI. Newly synthesized DNA was labeled with BrDU from HAEC cultured for 1 h on (C) laminin and (D) fibronectin (100 ×).

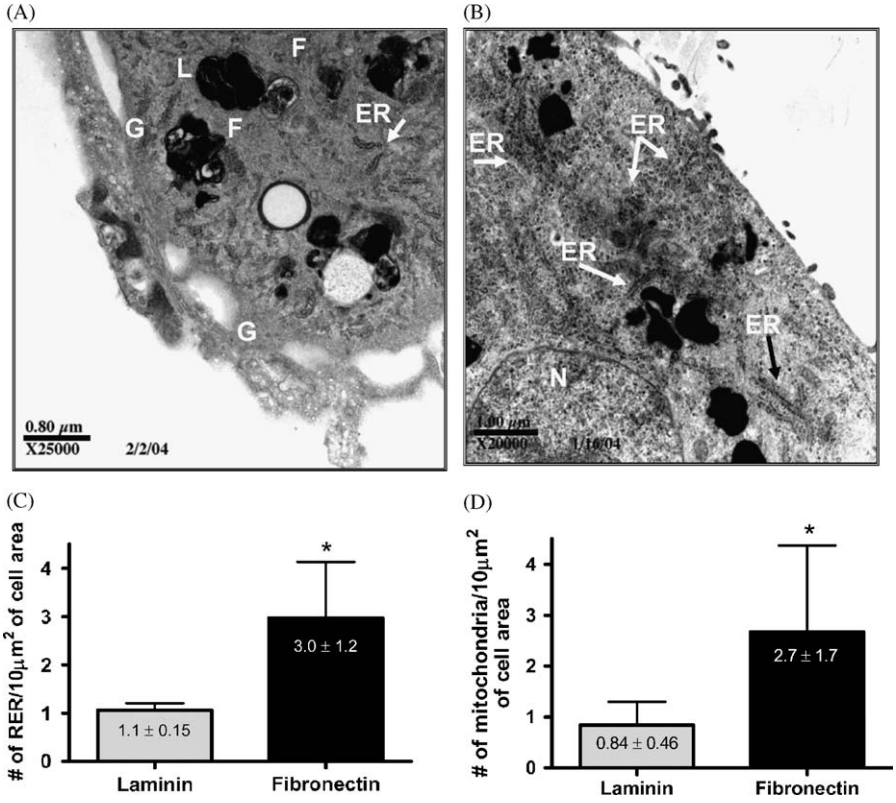

Fig. 4. Subcellular morphological observations were done with transmission electron microscopy (TEM) for SMCs cultured on (A) laminin and (B) fibronectin coated TCP. Representative images show the morphological differences between the two cell populations. G—Golgi network, F—filament, L—lysosomes, ER (with arrows)—endoplasmic reticulum, N—nucleus. Quantification of the number of (C) mitochondria and (D) rough endoplasmic reticulum (RER) observed per 10 μm^2 in TEM images ($n = 5$ images) at 12,000–40,000 × magnification. (*) indicates $p < 0.05$.

2.7. Statistical analysis

Numerical data were reported as a mean ± standard deviation. A student's 2-sample *t*-test was used to compare pairs of means. Analysis of variance (ANOVA) with post-hoc analysis using the Newman-Keuls multiple comparison test was used to determine significant differences among 3 or more means. A *p*-value of 0.05 or less was required for significance.

3. Results

3.1. Assessment of cell differentiation

SMC differentiation was confirmed with immunohistochemistry using phenotype specific markers. The contractile phenotype was confirmed in cells cultured on laminin, by the presence of abundant SM-α-actin (Fig. 3A). This result is in contrast to that of SMCs grown on fibronectin, where the staining of SM-α-actin is decreased (Fig. 3B). The results of the BrDU assay show that the cells grown on fibronectin are highly proliferative, when compared to the cells grown on laminin (Fig. 3C and D). Collectively, these data show that the substrates laminin and fibronectin synchronize the SMCs into the contractile and proliferative phenotype, respectively.

3.1.1. Microscopy

TEM images of the SMCs grown on each substrate show qualitative subcellular morphological differences. Representative TEM images have been selected to show that the

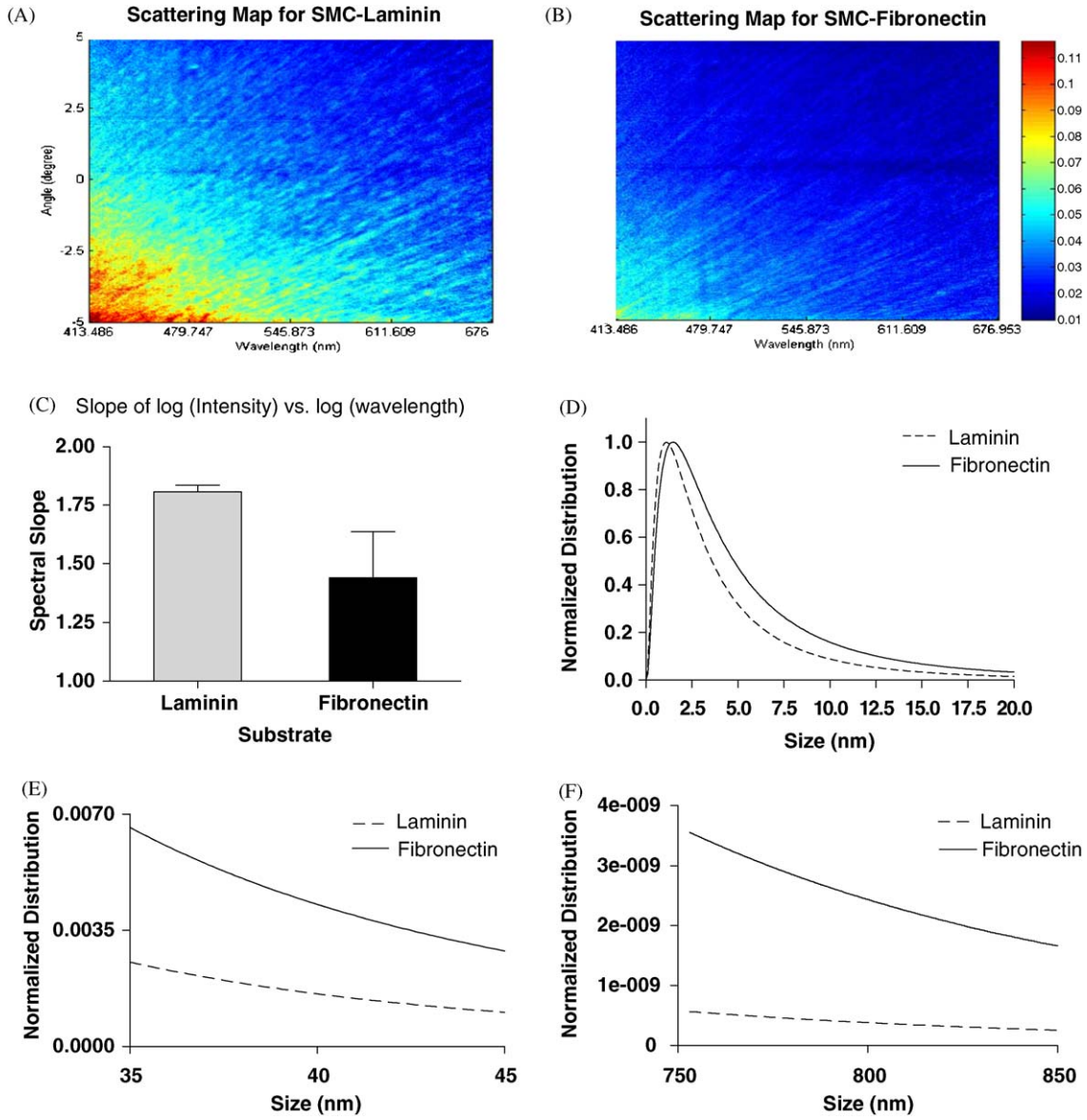

Fig. 5. 4D-ELF analysis of SMC phenotype on laminin and fibronectin-coated glass cover slips. Spectral "fingerprint" obtained of SMC cultured on (A) laminin, and (B) fibronectin. (C) The spectral slope data for cells cultured on laminin and fibronectin. Data are Mean ± SD, $N = 5$ and $p < 0.05$. (D) Normalized size distribution data show the shift in the size distribution of the cellular scattering components to the larger sized scatters of fibronectin. (E–F) Normalized distribution data at 40 and 800 nm.

cells in the proliferative phenotype had many organelles involved in proliferation such as extensive rough endoplasmic reticulum (ER), golgi stacks, and a large quantity of ribosomes (Fig. 4A). In contrast, the cells in the contractile phenotype had a greater amount of organelles required for contraction, such as extensive filament networks (Fig. 4B). Quantitative analysis of multiple TEM images shows that the SMC in the proliferative phenotype have significantly more mitochondria and RER relative to the SMC in the contractile phenotype (Fig. 4C and D).

3.1.2. 4D-ELF analysis

Based on the light-scattering analysis, there were significant subcellular morphological differences detected between the two SMC populations. Measurements were taken from at least 10 different positions within each glass cover slip containing subconfluent cells. From each set of measurements, a "fingerprint" is represented which depicts the intensity of the backscattered light across all wavelengths at backscattered angles $\pm 8^{\circ}$ (Fig. 5A and B). The spectral slope data are obtained by plotting the average intensity of the light at each wavelength over all backscattered angles (Fig. 5C). As mentioned previously, scattering intensity is a declining function of wavelength, and its slope is related to the relative proportion of structures of different sizes. Therefore, the mean slope and standard deviation (SD) of the log of the intensity vs. the log of the wavelength plots is represented. As described, "larger" structures tend to reduce the spectral slope, whereas "smaller" structures tend to increase the spectral slope. The proliferative SMC (cultured on fibronectin) have a smaller spectral slope as compared to the contractile SMCs (cultured on laminin) (Fig. 5C) (1.4 ± 0.2 and 1.8 ± 0.07, respectively; $p < 0.05$). This finding indicates that the proliferative SMCs have a greater proportion of larger sub-cellular structures when compared to the contractile SMCs. Representative size distribution profiles obtained from SMCs grown on laminin and fibronectin substrates suggest that the size distributions of SMCs grown on fibronectin shift towards larger sizes (40–800 nm, Fig. 5D–F). Furthermore, the relative portion of larger structures, the mean, and the most probable scatterers all become larger.

3.2. Assessment of cell adhesion

Endothelial cell attachment to fibronectin was faster and stronger than to laminin at each time point evaluated. Phase contrast images of ECs attached to laminin and fibronectin show increasing cell density as attachment time increases from 15 to 120 min (Fig. 6A). Additionally, a greater proportion of cells attach to fibronectin at each time point than to laminin. The data from the centrifugation assay show that at each time point, there are a greater percentage of cells that remain attached to fibronectin than to laminin (Fig. 6B). (15 min, laminin $5.1 \pm 1.6\%$, fibronectin $23.8 \pm 8.4\%$; 30 min, laminin $8.8 \pm 0.9\%$, fibronectin $64.9 \pm 6.7\%$; 60 min, laminin $32.1 \pm 9.2\%$, fibronectin $69.4 \pm 8.8\%$; 120 min laminin $33.9 \pm 0.4\%$, fibronectin $69.5 \pm 0.9\%$; $p < 0.05$ for all interactions). Furthermore, when cultured on fibronectin, the maximal force of attachment is reached by 30 min, with no statistical difference between the percent of cells attached for subsequent time points. In contrast, when cultured on laminin, the maximal force of attachment is reached by 60 min, with no statistical difference between the percent of cells attached for 60 or 120 min. Overall, there is a decrease in the rate and proportion of endothelial cell attachment when cultured on laminin vs. fibronectin.

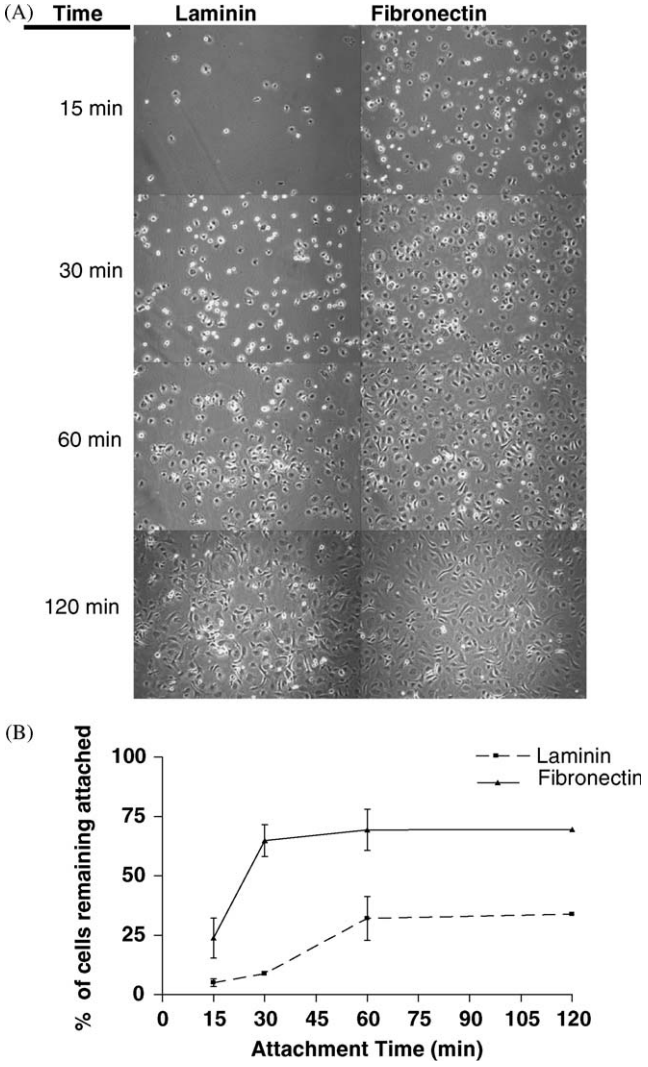

Fig. 6. EC attachment is time and substrate dependent. (A) Phase contrast images of ECs attached to laminin and fibronectin for 15–120 min. All images are $40\times$. (B) Centrifugation assay results showing HAEC force of attachment to laminin and fibronectin coated TCP. For all interactions the data represent Mean $\pm$ SD, $N = 3$, $p < 0.05$.

HAECs cultured on fibronectin form focal adhesion complexes in as early as 30 min as indicated by the green vinculin staining (Fig. 7A). The punctuate vinculin staining becomes more abundant and organized, localizing

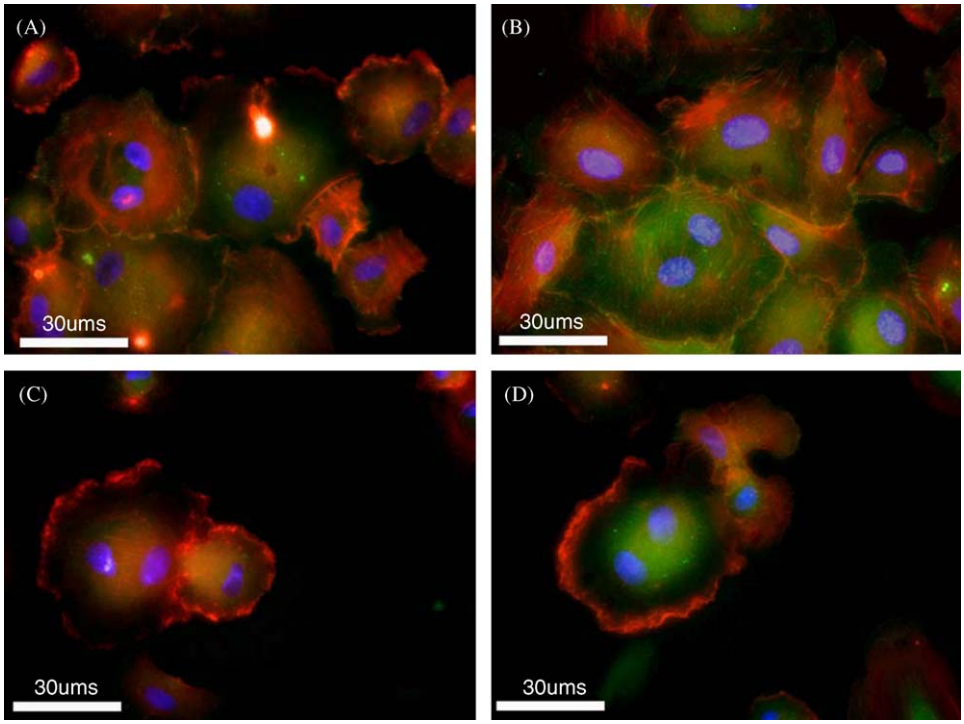

Fig. 7. Triple staining of HAECs for focal adhesion complex protein vinculin (green), and filamentous actin stain paxillin (red), and nuclei specific DAPI (blue). Triple-labeled HAECs cultured on fibronectin-coated TCP for (A) 30 min and (B) 120 min. Triple-labeled HAECs cultured on laminin-coated TCP for (C) 60 min and (D) 120 min. All images are 600 ×. Differences observed at these time points are in agreement with the differences in the 4D-ELF spectral slope.

throughout the body of the cell and at the cell periphery. The characteristic vinculin staining localizes to the site of actin stress fiber anchorage throughout the cell. There is a marked increase in the number of assembled focal adhesion complexes, and bundled actin filaments by 120 min in culture on fibronectin (Fig. 7B). This result is in contrast to the staining of HAECs cultured on laminin. The HAECs cultured on laminin show decreased expression of vinculin at 60 and 120 min in culture on laminin (Fig. 7C and D). Although vinculin expression increases in HAECs cultured on laminin by 120 min, the localization is still less organized and is diffuse throughout the cell, localizing primarily in the paranuclear region (Fig. 7D).

3.2.1. Microscopy

Representative TEM images of cells attached for 60 and 120 min to each substrate, laminin and fibronectin, show differences in cell attachment points and morphology of subcellular structures (Fig. 8). The representative TEM images of HAECs attached to fibronectin for 60 and 120 min reveal an increase in electron dense cell-substrate contact points (Fig. 8A and B arrows). The cells cultured on laminin for 60 and 120 min show a decrease or absence of these contact points (Fig. 8C and D). Additionally, the cytoplasm of HAECs attached to fibronectin and laminin for 60 min have an abundance of ribosomes, ER, mitochondria, and golgi complex structures. In contrast, when the cells are attached for 120 min to laminin and fibronectin, there is a decrease in the abundance of these organelles. This decrease is more pronounced in cells cultured on fibronectin than on laminin. Quantitative analyses of multiple TEM images reveal the density of the electron dense contact points (Fig. 8E). These results show that the cells attached to fibronectin for 60 min have a significantly greater density of contact points per 10 μm of cell length, as compared to the cells attached to laminin for the same time (laminin 60 min 3.7 ± 1.1; fibronectin 60 min 8.8 ± 1.0). Additionally, there is a significant increase in the number of contact points in cells cultured on laminin from 60 to 120 min (laminin 60 min 3.7 ± 1.1; laminin 120 min 8.3 ± 1.7). There is no difference in the number of contact points present on cells attached to fibronectin for 60–120 min (fibronectin 60 min 8.8 ± 1.0; fibronectin 120 min 9.4 ± 2.5). These representative TEM images and the quantitative data demonstrate that there are changes in the abundance of electron dense cell/substrate contact points, as well as the changes in the subcellular organelle distribution as cells interact with both substrates over time.

3.2.2. 4D-ELF analysis

HAECs at various degrees of attachment were analyzed via 4D-ELF for changes in the subcellular morphology of the cells as attachment to laminin and fibronectin progresses. As the HAECs attach to each substrate, at most time points, the spectral slope is significantly higher for the cells attached to fibronectin as compared to the slope obtained for cells attached to laminin (Fig. 9) (15 min, laminin 0.93 ± 0.19, fibronectin 1.21 ± 0.14, $p < 0.05$; 30 min,

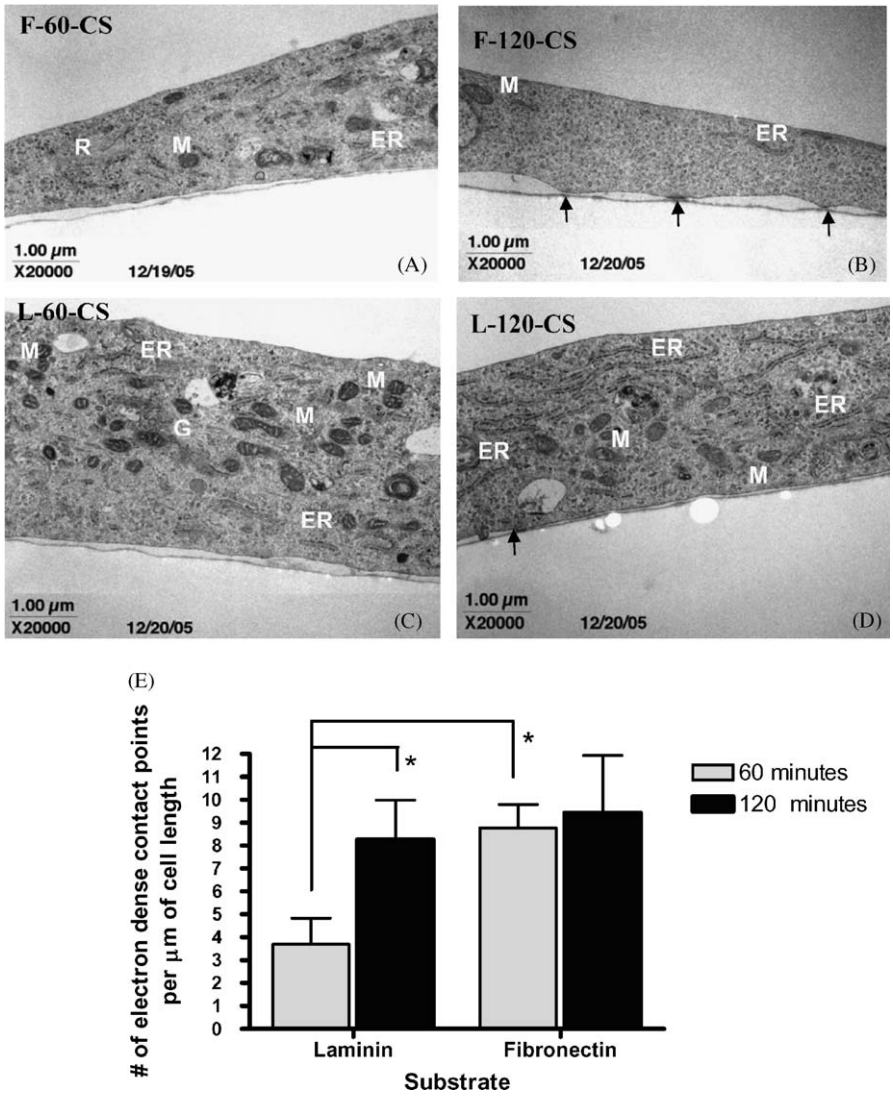

Fig. 8. Subcellular morphological observations were done with transmission electron microscopy (TEM) of HAECs cultured on fibronectin for (A) 60 min and (B) 120 min and laminin for (C) 60 min and (D) 120 min. Representative images show the morphological differences between HAECs attached to each surface for each amount of time. R—ribosomes, M—mitochondria, ER—endoplasmic reticulum, G—Golgi, arrows—electron dense substrate contact points. (E) Quantification of electron dense contact points from a subset of TEM images for ECs cultured on laminin for 60 ($n = 8$ images) and 120 min ($n = 4$ images), and fibronectin for 60 ($n = 5$ images) and 120 min ($n = 7$ images) at 20,000–40,000 × magnification. (*) indicates $p < 0.05$.

laminin 1.12 ± 0.19, fibronectin 1.29 ± 0.07, $p > 0.05$; 60 min, laminin 1.15 ± 0.16, fibronectin 1.56 ± 0.29, $p < 0.05$; 120 min laminin 1.55 ± 0.2, fibronectin 1.83 ± 0.016, $p < 0.05$). Based on the spectral slopes of HAEC grown on laminin and fibronectin, the size of the scattering particles within the cells is smaller and larger, respectively.

3.3. Assessment of cell apoptosis

3.3.1. LDH release and morphology evaluation via microscopy

The later stage of apoptosis involving the loss of plasma membrane integrity of HAECs was assessed via release of cytoplasmic LDH. Following exposure to 0.10, 0.5, 1.0, 10 and 50 ng/ml TNF-α, there is an increasing amount of LDH released into the media that corresponds to increasing TNF-α concentration. There is no significant difference in the amount of LDH released into the culture media upon exposure to the three lowest concentrations of TNF-α, 0.10, 0.5 and 1.0 ng/ml as compared to the baseline amount of LDH (Fig. 10A) (0.1052 ± 0.04, 0.1235 ± 0.05, 0.179 ± 0.08, respectively $p > 0.05$). In contrast, when the concentration of TNF-α is increased to 10 and 50 ng/ml, there is a significant increase in LDH released, indicating plasma membrane damage, when compared to control cells not exposed to TNF-α (0.227 ± 0.10, 0.314 ± 0.14, respectively $p < 0.05$). When compared to cells not exposed to TNF-α, light microscopy images show that there is no observable difference in the cell morphology when cells are exposed to no TNF-α, 0.10 and 0.50 ng/ml TNF-α (Fig. 10B–D, respectively). Conversely there is a marked difference in the cell morphology of cells exposed to 50 ng/ml TNF-α. It

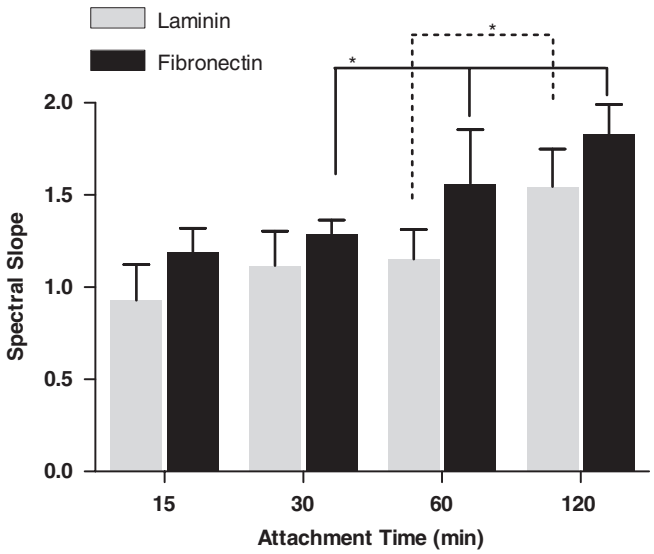

Fig. 9. 4D-ELF analysis of HAECs cultured on glass cover slips coated with fibronectin and laminin for 15, 30, 60 and 120 min. Data are Mean ± SD, $N = 12$, (*) indicate data that are statistically different $p < 0.05$.

is clear that the plasma membrane is severely compromised (Fig. 10E).

3.3.2. Caspase-3 activity

There is no significant difference in caspase-3 activity between cells incubated with no TNF-α and those incubated with 0.1 ng/ml TNF-α (54.8 ± 15.9 U/ml, 71.1 ± 22.1 U/ml, respectively $p > 0.05$) (Fig. 11). However, when HAECs were exposed to 0.5 ng/ml TNF-α for 3 h, the molecular cascades present during the early stage of apoptosis were activated causing a significant increase in the caspase-3 activity (54.8 ± 15.9 U/ml vs. 86.6 ± 28.6 U/ml, $p < 0.05$) (Fig. 11). These results show that the early molecular events of apoptosis are initiated upon exposure of HAECs to 0.5 ng/ml TNF-α for 3 h. These early events eventually lead to obvious morphological changes; however, within the experimental time frame set here, no observable morphological changes have occurred.

3.3.3. Endothelial cell apoptosis 4D-ELF analysis

HAECs undergoing the early biochemical events of apoptosis were analyzed via 4D-ELF for nanoscale changes in subcellular morphology. Based on the spectral slope data, there is a significant difference in the subcellular morphology of HAECs that correspond with exposure to the apoptosis inducing cytokine TNF-α for 3 h (Fig. 12). The spectral slope of uninduced HAECs is 3.0 ± 0.9 whereas the slopes of cells exposed to 0.10 and 0.50 ng/ml TNF-α are 1.9 ± 0.9 and 1.8 ± 0.2, respectively ($p < 0.05$). As the early biochemical events of apoptosis are occurring, although undetectable with conventional microscopy, there is a change in the subcellular morphology of the cells that can be detected with the sensitive method of 4D-ELF.

4. Discussion

Many bio-optics techniques have been shown to be useful in detecting tissue micro-architecture. We describe for the first time, the use of a novel comprehensive optical technique referred to as 4D-ELF for the assessment of cell-material interactions. Herein it is reported that 4D-ELF can be used for the non-invasive assessment of SMC and HAEC structural differences associated with processes such as differentiation, proliferation, substrate attachment, and the early stages of apoptosis. The application of this system is ideal for high-throughput screening of cell–material interactions. In a tightly controlled environment where known process and cell changes are to be assessed, the system once calibrated can provide a means to quantitatively detect these changes. The structural changes that accompany each cell process described, and the corresponding effect on the 4D-ELF spectral slope data is shown in Table 1. It is clear that for each process there is an anticipated change in the 4D-ELF spectral data.

SMCs were used as an initial model system to assess the ability of 4D-ELF to detect nanoscale structural characteristics that accompany phenotypic modulation. As SMCs grow they can undergo a reversible conversion in their phenotype from proliferative/synthetic to differentiated/contractile [21,23]. This conversion from contractile to proliferative involves marked structural changes that include the loss of an abundant actin and myosin structures, an increase in the number and size of synthetic organelles such as ER, mitochondria, and golgi complex. 4D-ELF is sensitive to scatterers in the size range of 40–800 nm. Based on the size distribution data, for SMCs grown on fibronectin the most probable sizes of the scatterer all become larger and more abundant as compared to the SMCs grown on laminin. The statistically significant differences in the spectral slopes indicate that this parameter may be used to monitor the cellular structural changes in a population of cells cultured on biomaterials, especially if screening for populations of cells that are differentiated on a material of interest.

TEM analysis confirms the above-described structural characteristics for SMCs in the contractile and proliferative phenotype and allows the identification of the organelles or structures that undergo morphological changes. The ER is composed of tubules whose outer diameter ranges from 30 to 100 nm, the overall thickness of Golgi apparatus can range from 100 to 400 nm, and mitochondria vary in overall size, but can be as small as 0.5 μm [11,34]. The ER and golgi are organelles that have been shown to undergo changes in size, abundance, and distribution as cells shift between the two phenotypes [24,25]. The sizes of these organelles are within 40–800 nm, which corresponds to the range of sensitivity of the light scattering spectrum [6]. We suggest that the "light-scattering particles" in this case are subcellular organelles and structures that undergo changes in size and distribution that correspond with the two distinct SMC phenotypes. Therefore, we report that the

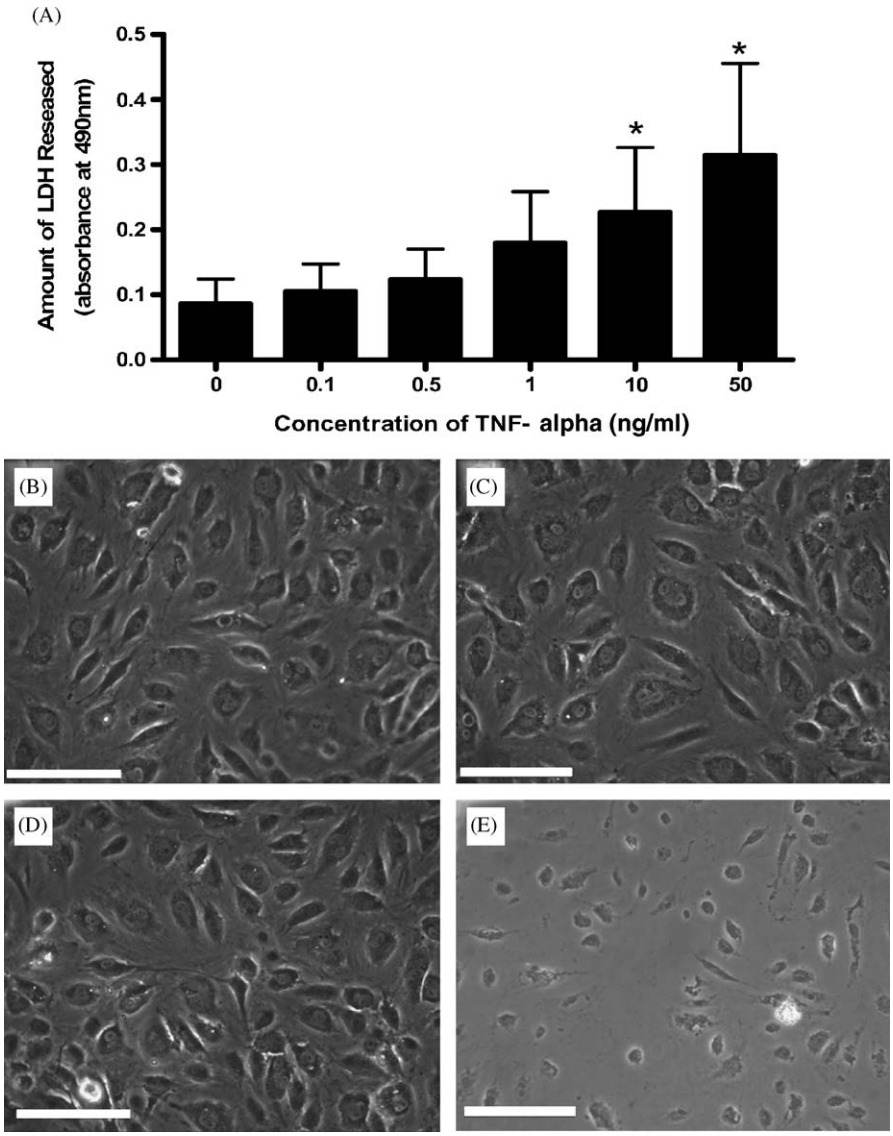

Fig. 10. Detection of apoptosis by measure of LDH. (A) Release of intracellular LDH from HAECs cultured without TNF-α (baseline control) or 0.10, 0.50, 1.0, 10 and 50 ng/ml. Data are Mean ± SD, $N = 8$, (*) indicates $p < 0.05$ as compared to the baseline control. Phase contrast images of HAECs cultured for 3 h in (B) no TNF-α, (C) 0.1 ng/ml, (D) 0.5 ng/ml and (E) 50 ng/ml TNF-α. Images show the morphology of the cells following 3 h of exposure to TNF-α (scale bar = 100 ums).

method of 4D-ELF is sensitive enough to detect subtle changes in sub-cellular organelle size and distribution, such that it can be used to distinguish between smooth muscle cells in the contractile and proliferative phenotypes.

These studies were also extended to endothelial cells. Both angiogenesis and in vitro behavior of endothelial cells are complex phenomena with multiple progressive steps toward new blood vessel formation. One of the earliest steps in the pathway to tissue formation is endothelial cell adhesion and retention to the substrate. Cell adhesion is mediated by integrin receptors triggering several pathways leading to cytoskeletal changes of the myosin and actin filaments, as well as the recruitment and assembly of focal adhesion complexes [20,35]. As HAECs attach and interact with substrates, there is an immediate morphological response that involves cytoskeletal structural components that affect the shape of the cells as they shift from being round in suspension to flat and spread onto the surface. There is also an immediate recruitment of a matrix of proteins involved in anchoring the cell to the surface, by way of focal adhesion complexes [20]. As endothelial cells go from round to spread during substrate attachment there is a well-characterized effect on the size and shape of the nucleus, causing it to "deform" [17]. Additionally, during cell attachment, there are forces exerted by the cytoplasmic filaments that can cause the subcellular organelles to rearrange and/or redistribute [16]. These subcellular changes may give rise to light-scattering spectroscopic fingerprints that can be used to describe the degree of attachment of the cell population once calibrated against attachment standards. This 4D-ELF fingerprint represents a population of cells and is not affected by cell density.

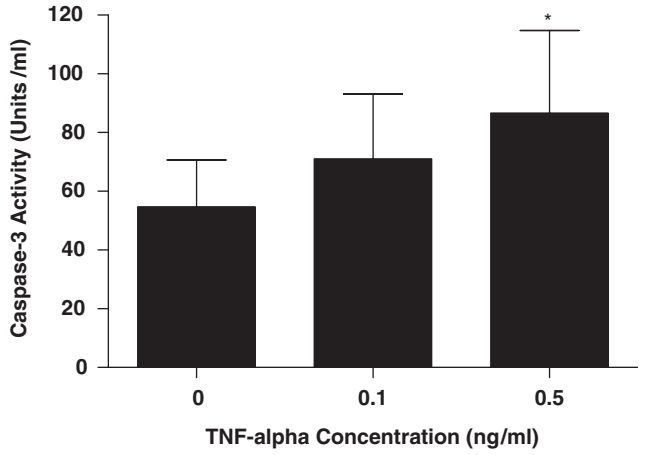

Fig. 11. Caspase-3 activity was measured from cell lysates of HAECs cultured without TNF-α (baseline control, $N = 6$), or with 0.10 ng/ml ($N = 7$) and 0.5 ng/ml ($N = 9$) TNF-α challenge. Data was converted to Units/ml for each sample. Data are Mean ± SD, (*) indicates $p < 0.05$ when compared to the baseline activity.

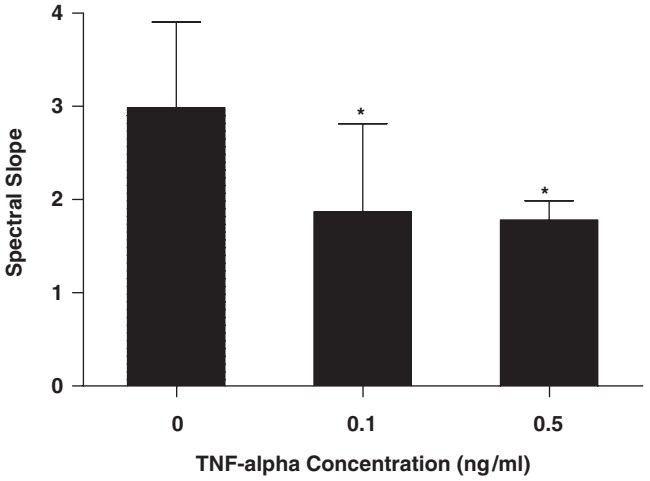

Fig. 12. 4D-ELF data of HAECs cultured on glass cover slips undergoing apoptosis in response to no TNF-α ($N = 9$), 0.10 ng/ml ($N = 10$) and 0.5 ng/ml ($N = 7$) TNF-α exposure. Data are Mean ± SD. (*) indicates $p < 0.05$ as compared to the spectral slope of the control (no TNF-α).

The 4D-ELF data are in agreement with the degree of attachment of the HAECs assessed via the centrifugation assay, as well as the assembly of focal adhesion complexes in HAECs attached to each substrate. We confirm previous reports that EC attachment to protein-coated surfaces is time and substrate dependent with overall stronger and faster attachment to fibronectin than to laminin [36,37]. In addition to differences in focal adhesion complex formation and abundance, there are also changes in the cytoplasmic organelle distribution and composition in cells attached to laminin and fibronectin. As the EC attachment time increases from 60 to 120 min, there is a decrease in the abundance of ribosomes, ER, mitochondria, and golgi complex structures. These structural differences are represented in the 4D-ELF spectral data, whereby the spectral slope increases for HAECs attached to both substrates over time; indicating that size of the scattering organelles are decreasing and/or becoming less abundant.

The representative TEM images demonstrate qualitatively that there are changes in the number, size, and abundance on electron dense cell/substrate contact points, as well as the changes in the subcellular organelle distribution as cells interact with both substrates over time. Therefore, 4D-ELF is also sensitive enough to detect changes in the subcellular morphology of EC at varying degrees of attachment to laminin and fibronectin. It is likely that 4D-ELF is detecting changes that accompany the assembly of an organized actin network and/or focal adhesion complex formation.

The EC attachment study allows the assessment of cell density on the 4D-ELF fingerprint. If the 4D-ELF measurements were simply detecting an increase in cell number, the fingerprints (regardless of substrate) would reflect a progressively decreasing slope over time to account for the detection of increasing numbers of large scatterers, in this case individual cells. This is not the case, as the density of attached cells increases over attachment time to each substrate, the 4D-ELF fingerprints are not affected in this way. Instead, 4D-ELF assesses subcellular structural changes that are occurring in a population of cells found within the 1 mm diameter of illuminated light.

Table 1
Summary of expected changes in subcellular structures and 4D-ELF signals

Cell process	Subcellular changes	4D-ELF spectral changes
Proliferative SMC	Increased size and abundance of synthetic organelles (RER, golgi, mitochondria)	Decrease slope[a] (i.e.—greater no. of "large" scatterers)
Contractile SMC	Decreased size and abundance of synthetic organelles (RER, golgi, mitochondria)	Increased slope[b] (i.e.—greater no. of "smaller" scatterers)
EC attachment	Increase in focal adhesion	Increased slope[c] (i.e.—greater no. of "smaller" scatterers)
EC apoptosis	Chromatin condensation	Decreased slope[d] (i.e.—greater no. of "large" scatterers)

[a]This decreased slope is relative to contractile SMCs in the study described herein.
[b]This increase in slope is relative to proliferative SMCs in the study described herein.
[c]This increased slope is reflected over time from 15–120 min and corresponds with increasing attachment in the study described herein.
[d]This decreased slope is relative to cells that are not undergoing apoptosis as in the study described herein.

For these analyses, the measurement is repeated multiple times and the intensity signals are average to provide information about the population of cells, rather than just one individual cell.

Lastly, the process of apoptosis of HAECs was assessed. Upon receiving specific signals instructing a cell to undergo apoptosis, a number of distinctive biochemical and morphological changes occur. A method to non-invasively detect the onset of apoptosis is a valuable tool for use in the study of cell/material interactions. The 4D-ELF data show that there are differences in the size distributions of subcelluar structures of cells induced to undergo apoptosis. The changes that were detected via 4D-ELF are changes that are not easily observed. Measurement of released LDH indicates that the cell membrane was intact at the time of the 4D-ELF measurements. This finding is further supported by the phase contrast images of the cells demonstrating no visible change in cell morphology. To confirm the onset of the molecular events of apoptosis, caspase-3 activity was measured. There is an increase in caspase-3 activity following exposure to 0.5 ng/ml TNF-α, indicating that the biochemical process of apoptosis has begun, and 4D-ELF could detect this onset by quantifying differences in the sub-cellular characteristics of the cells.

5. Conclusions

4D-ELF has many advantages over other techniques used to obtain structural information including: safety (as it uses low intensity visible light); non-perturbing measurements, (no need for chemical fixation as live cells can be analyzed) and quantitation (mathematical parameters can be obtained from the data to enable quantitative comparison). Also, it allows for quantitative measurements in real time. This method of assessing cell–material interactions is not without its limitations, at present this system is ideal for very controlled environments where one process is being assessed at a time, as the system can be calibrated for specific process detection. The spectral slope described herein is one tool that can be obtained non-invasively to assess a cell process that is occurring in a population of cells. Nonetheless, we have shown that 4D-ELF provides an otherwise unattainable insight into the nano-scale architecture of living cells and tissue organization. As cells attach to engineered scaffolds, and begin to proliferate and integrate, 4D-ELF can potentially be used to monitor these events in real time, non-invasively.

Acknowledgments

J. Allen was supported by a NIH Biotechnology Training Grant Program (Grant # 2T32GM008449-11). The authors thank the National Institutes of Health, National Heart Lung and Blood Institute grant number R21 HL071921-03 for financial support of this work. Additionally, we thank HyungJoo Yoon for her technical support in obtaining 4D-ELF measurements.

References

[1] Hug TS. Biophysical methods for monitoring cell–substrate interactions in drug discovery. Assay Drug Dev Technol 2003;1(3):479–88.
[2] Drexler W, Morgner U, Kartner FX, Pitris C, Boppart SA, Li XD, et al. In vivo ultrahigh-resolution optical coherence tomography. Opt Lett 1999;1, 24(17):1221–3.
[3] Notingher I, Verrier S, Romanska H, Bishop AE, Polak JM, Hench LL. In situ characterisation of living cells by Raman spectroscopy. Spectrosc-Int J 2002;16(2):43–51.
[4] Verrier S, Notingher I, Polak JM, Hench LL. In situ monitoring of cell death using Raman microspectroscopy. Biopolymers 2004; 74(1–2):157–62.
[5] Wax A, Yang CH, Backman V, Badizadegan K, Boone CW, Dasari RR, et al. Cellular organization and substructure measured using angle-resolved low-coherence interferometry. Biophys J 2002;82(4): 2256–64.
[6] Roy HK, Liu Y, Wali RK, Kim YL, Kromine AK, Goldberg MJ, et al. Four-dimensional elastic light-scattering fingerprints as preneoplastic markers in the rat model of colon carcinogenesis. Gastroenterology 2004;126(4):1071–81.
[7] Backman V, Gurjar R, Badizadegan K, Itzkan L, Dasari RR, Perelman LT, et al. Polarized light scattering spectroscopy for quantitative measurement of epithelial cellular structures in situ. IEEE J Sel Top Quant 1999;5(4):1019–26.
[8] Backman V, Gopal V, Kalashnikov M, Badizadegan K, Gurjar R, Wax A, et al. Measuring cellular structure at submicrometer scale with light scattering spectroscopy. IEEE J Select Topics Quantum Electron 2001;7(6):887–93.
[9] Gurjar RS, Backman V, Perelman LT, Georgakoudi I, Badizadegan K, Itzkan I, et al. Imaging human epithelial properties with polarized light-scattering spectroscopy. Nat Med 2001;7(11):1245–8.
[10] Backman V, Wallace MB, Perelman LT, Arendt JT, Gurjar R, Muller MG, et al. Detection of preinvasive cancer cells. Nature 2000;6, 406(6791):35–6.
[11] Boustany NN, Kuo SC, Thakor NV. Optical scatter imaging: subcellular morphometry in situ with Fourier filtering. Opt Lett 2001; 26(14):1063–5.
[12] Boustany NN, Tsai YC, Pfister B, Joiner WM, Oyler GA, Thakor NV. BCL-x(L)-dependent light scattering by apoptotic cells. Biophys J 2004;87(6):4163–71.
[13] Hulst HCvd. Light scattering by small particles. N.Y.: Dover Publications; 1981.
[14] Ingber DE. Fibronectin controls capillary endothelial cell growth by modulating cell shape. Proc Natl Acad Sci USA 1990;87(9):3579–83.
[15] Christopher RA, Judge SR, Vincent PA, Higgins PJ, McKeown-Longo PJ. The amino-terminal matrix assembly domain of fibronectin stabilizes cell shape and prevents cell cycle progression. J Cell Sci 1999;112(Part 19):3225–35.
[16] Ausprunk DH, Berman HJ. Spreading of vascular endothelial cells in culture: spatial reorganization of cytoplasmic fibers and organelles. Tissue Cell 1978;10(4):707–24.
[17] Jean RP, Gray DS, Spector AA, Chen CS. Characterization of the nuclear deformation caused by changes in endothelial cell shape. J Biomech Eng 2004;126(5):552–8.
[18] Dejana E, Colella S, Languino LR, Balconi G, Corbascio GC, Marchisio PC. Fibrinogen induces adhesion, spreading, and microfilament organization of human endothelial cells in vitro. J Cell Biol 1987;104(5):1403–11.
[19] Reinhart-King CA, Dembo M, Hammer DA. The dynamics and mechanics of endothelial cell spreading. Biophys J 2005;89(1): 676–89.
[20] Christopher RA, Kowalczyk AP, McKeownLongo PJ. Localization of fibronectin matrix assembly sites on fibroblasts and endothelial cells. J Cell Sci 1997;110:569–81.
[21] Hedin U, Sjolund M, Hultgardhnilsson A, Thyberg J. Changes in expression and organization of smooth-muscle-specific alpha-actin

during fibronectin-mediated modulation of arterial smooth-muscle cell phenotype. Differentiation 1990;44(3):222–31.
[22] Hu WY, Fukuda N, Satoh C, Jian T, Kubo A, Nakayama M, et al. Phenotypic modulation by fibronectin enhances the angiotensin II-generating system in cultured vascular smooth muscle cells. Arterioscler Thromb Vasc Biol 2000;20(6):1500–5.
[23] Worth NF, Rolfe BE, Song J, Campbell GR. Vascular smooth muscle cell phenotypic modulation in culture is associated with reorganisation of contractile and cytoskeletal proteins. Cell Motil Cytoskeleton 2001;49(3):130–45.
[24] Thyberg J. Caveolae and cholesterol distribution in vascular smooth muscle cells of different phenotypes. J Histochem Cytochem 2002; 50(2):185–95.
[25] Thyberg J. Phenotypic modulation of smooth muscle cells during formation of neointimal thickenings following vascular injury. Histol Histopathol 1998;13(3):871–91.
[26] Thyberg J, Hultgardh-Nilsson A. Fibronectin and the basement membrane components laminin and collagen type IV influence the phenotypic properties of subcultured rat aortic smooth muscle cells differently. Cell Tissue Res 1994;276(2): 263–71.
[27] Suarez-Huerta N, Lecocq R, Mosselmans R, Galand P, Dumont JE, Robaye B. Myosin heavy chain degradation during apoptosis in endothelial cells. Cell Proliferat 2000;33(2):101–14.
[28] Schwartzman RA, Cidlowski JA. Apoptosis—the biochemistry and molecular-biology of programmed cell-death. Endocr Rev 1993;14(2): 133–51.
[29] Reyes CD, Garcia AJ. A centrifugation cell adhesion assay for high-throughput screening of biomaterial surfaces. J Biomed Mater Res A 2003;67(1):328–33.
[30] Robaye B, Mosselmans R, Fiers W, Dumont JE, Galand P. Tumor-necrosis-factor induces apoptosis (programmed cell-death) in normal endothelial-cells in vitro. Am J Pathol 1991;138(2):447–53.
[31] Chang SY, Roy HK, Kim Y, Liu Y, Goldberg MJ, Wali RK, et al. Four-dimensional elastic light-scattering fingerprinting (4D-ELF) provides accurate risk stratification for human colonic neoplasia. Gastroenterology 2004;126(4):A342-a.
[32] Kim YL, Liu Y, Wali RK, Roy HK, Goldberg MJ, Kromin AK, et al. Simultaneous measurement of angular and spectral properties of light scattering for characterization of tissue microarchitecture and its alteration in early precancer. IEEE J Sel Top Quant 2003;9(2): 243–56.
[33] Borse GJ. FORTRAN 77 and numerical methods for engineers. 2nd ed. Boston: PWS-KENT Publishing Co.; 1991.
[34] Bozzola JJ. Electron microscopy: principles and techniques for biologist. 2nd ed. Sudbury: Jones and Bartlett; 1999.
[35] Short SM, Talbott GA, Juliano RL. Integrin-mediated signaling events in human endothelial cells. Mol Biol Cell 1998;9(8):1969–80.
[36] Consigny PM, Vitali NJ. Resistance of freshly adherent endothelial cells to detachment by shear stress is matrix and time dependent. J Vasc Interv Radiol 1998;9(3):479–85.
[37] Pratt KJ, Jarrell BE, Williams SK, Carabasi RA, Rupnick MA, Hubbard FA. Kinetics of endothelial cell-surface attachment forces. J Vasc Surg 1988;7(4):591–9.